Marine and Petroleum Geology 110 (2019) 21–34

Contents lists available at ScienceDirect

Marine and Petroleum Geology

journal homepage: www.elsevier.com/locate/marpetgeo

Research paper

Mass transfer between mudstone-sandstone interbeds during diagenesis as revealed from the type and distribution of carbonate cements in the Eocene beach-bar sandstones, Bohai Bay Basin

Jian Wang[a,b,*], Yingchang Cao[a,b,**], Keyu Liu[a,c], Xintong Wang[a], Jie Xiao[a], Ning Xie[a]

[a] School of Geosciences, China University of Petroleum (East China), Qingdao 266580, China
[b] Key Laboratory of Deep Oil & Gas Geology and Geophysics China (University of Petroleum), Ministry of Education, Qingdao 266580, China
[c] Department of Applied Geology, Curtin University, GPO Box U1987, Perth, WA 6845, Australia

ARTICLE INFO

Keywords:
Carbonate cement
Carbon and oxygen isotope
Mass transfer
Material source
Beach-bar
Dongying depression

ABSTRACT

The characteristics, heterogeneous distribution and origins of carbonate cements within beach-bar sandstones in the Boxing Sag and implications on the mass transfer from mudstone to sandstone during diagenetic process was investigated systematically by an integrated analysis invoking petrography, carbon and oxygen stable isotopes and porosity-permeability, with specific references to the contrasts among the sharp (S)-change lithology (S-mudstone-S-sandstone interbeds), the gradual (G) -change lithology (G-mudstone-G-sandstone interbeds) and the center of sandstones. There are distinct differences in the occurrence, content, distribution, carbon and oxygen isotopic compositions and precipitation temperatures of the carbonate cements among the S-sandstone, G-sandstone and center of sandstone. Material sources of carbonate cements in the S-sandstones are mainly derived from the diagenetic alterations of the nearby S-mudstones through mass transfer with the participation of organic CO_2, while in the G-sandstones, the material sources are mainly internal and originated from the calcareous matrix. Dissolution of feldspars and conversion of clay minerals provided the main materials for the precipitation of carbonate cements in the center of sandstones. Mass transfer of carbonate cements mainly occurred between the S-mudstones and the S-sandstones with limited transmission distance, which controlled the distribution of carbonate cements in the S-mudstones. There was almost no mass transfer between the G-mudstones and G-sandstones because of the small concentration gradient, instead, the depositional components and recrystallization controlled the carbonate distribution of the G-sandstones.

1. Introduction

Carbonates are common in the clastic rock reservoirs and constitute an important authigenic mineral, which is widely distributed and can be formed by various mechanisms during the diagenetic process (Rossi et al., 2001; Mansour et al., 2014). Carbonate cements may form tight layers in sandstones during the diagenetic process. Tight carbonate cemented layers occur extensively in clastic reservoirs with the common distribution locations are near the sandstone-mudstone contacts (Boles and Franks, 1979; Dos Anjos et al., 2000; Wang et al., 2016, 2017a,b, 2019), in the high porosity-permeability zones of sandstones (Dos Anjos et al., 2000; Dutton et al., 2002; Fayek et al., 2001; Dutton, 2008), at the bottom of the sedimentary sequences (McBride et al., 1995), near the oil-water interfaces (De Souza and De Assis Silva, 1998), and at the boundary of phreatic zone and vadose zone (El-Ghali et al., 2013). Carbonate cements in these tight sandstone layers have many potential sources, such as internal, external, or mixed source (Dutton, 2008). The internal sources are mainly carbonate grains and cements in the sandstone itself, including biological debris, carbonate rock fragments, and calcareous matrix, etc. (Milliken et al., 1998; Dutton, 2008), and the external sources are mainly from the out part of the sandstone through mass transfer during the diagenesis (Schultz et al., 1989; Lynch and Land, 1996; Wang et al., 2016, 2018).

Sedimentary characteristics of sandstones, such as depositional facies, grain size, sorting, content of matrix, and sedimentary sequence, affect the diagenetic process and the distribution of diagenetic products to a great extent (Rossi et al., 2002; Karim et al., 2010; Zhang et al., 2012). More attention has been paid on the distribution of diagenetic alteration within depositional facies in recent years (El-Ghali et al., 2006, 2009; Kordi et al., 2011; Mansurbeg et al., 2012). Clastic

* Corresponding author. School of Geosciences, China University of Petroleum, Qingdao, Shandong 266580, China.
** Corresponding author. School of Geosciences, China University of Petroleum East China, Qingdao 266580, China.
E-mail addresses: wangjian8601@upc.edu.cn (J. Wang), caoych@upc.edu.cn (Y. Cao).

https://doi.org/10.1016/j.marpetgeo.2019.07.005
Received 18 April 2018; Received in revised form 28 June 2019; Accepted 2 July 2019
Available online 09 July 2019
0264-8172/

depositions, especially the sandstone and mudstone intervals, usually show the sudden change or gradual change of the lithology variation between sandstone and mudstone (Holail et al., 2006). The contact of sandstone and mudstone is an active area of water-rock interactions (Loyd et al., 2012). Many researchers have noted that diagenesis in sandstones was affected apparently by the reactions in adjacent mudstones through mass transfer (Fontana et al., 1986; Shew, 1990; McMahon et al., 1992; Gaupp et al., 1993; Macaulay et al., 1993; Hesse and Abid, 1998; Thyne, 2001; Dutton, 2008; Wang et al., 2016, 2018, 2019). The sudden change and the gradual change of sedimentation causes the differences of compositions and structures of sandstones and mudstones, which may contribute the differences of mass transfer and diagenetic process, but there was nearly no literature to discuss the influences on mass transfer and corresponding diagenesis from the types of lithology variation between sandstone and mudstone.

The beach-bar intervals in the Boxing Sag, Bohai Bay Basin are the typical deposits of sandstone interbedded with mudstone frequently with sudden and gradual lithology changes between sandstones and mudstones (Jiang et al., 2011). Preliminary study shows that carbonate cements are the majority authigenic minerals and various types of carbonate cements occur in beach-bar sandstones (Wang et al., 2017b, 2019). This study aims to elucidate and discuss the differences of the origin and distribution of carbonate cements and their implications for mass transfer from mudstones to sandstones through an integrated analysis of petrology, mineralogy, carbon and oxygen isotope ratios of carbonate cements.

2. Geological background

The Bohai Bay Basin is an important hydrocarbon producing basin in eastern China, covering an area of approximately 200,000 km^2. The basin is a complex rifted basin that formed in the Late Jurassic through the early Tertiary on the basement of the North China platform. The tectonic evolution of the basin consists of a synrift stage (65.0–24.6 Ma) and postrift stage (24.6 Ma to present) (Lampe et al., 2012). The Bohai Bay Basin consists of several subbasins (Fig. 1A). The Dongying Depression is a secondary tectonic unit of the Jiyang Subbasin and the Boxing Sag is a secondary tectonic unit of the Dongying Depression consisting of the Gaoqing fault in the west, Shicun fault in the east, Chunhua-Caoqiao fault in the north and Luxi Uplift in the south (Fig. 1B). The Boxing-1 and Boxing-2 faults are two second-order faults in the center of the Boxing sag (Jiang et al., 2011).

The Boxing Sag developed on a northward-dipping, subsiding, faulted block within the Dongying Depression (Fig. 1B). The sag is filled with Cenozoic to Quaternary deposites, which are composed of the Kongdian (Ek), Shahejie (Es), Dongying (Ed), Guantao (Ng), Minghuazhen (Nm) and Pingyuan (Qp) formations. From the base to the top the Es formation can be divided into four members, which are Es4, Es3, Es2 and Es1, respectively (Fig. 2). The upper part of the Es4 member (Es4s) consists of fine-grained and thin-bedded sandstones interbedded with gray mudstone, which is the focus of this study. The Es4s member developed during the late period of the initial rift stage, which can be divided into the Es4s lower and the Es4s upper. During the sedimentary stage of the Es4s lower, large-scale shore-shallow beach-bar sandbodies developed under the conditions of gentle paleotopography, a shore-shallow lacustrine environment and a relative abundance of sediment supply (Jiang et al., 2011). During the sedimentary stage of the Es4s upper, large-scale dark-gray mudstones and shale developed, which are some of the major hydrocarbon source rocks in the Boxing Sag (Guo et al., 2014). Analyses of logging, seismic and core data indicate that the beach-bar sandstones in the Boxing Sag trend NE-SW with a mat shape (Jiang et al., 2011). The strata, which are characterized by sandstone and mudstone interval layers, are up to 200 m thick (Wang et al., 2017a). The beach-bar sandstones is usually buried between the depth of 2300 and 3500 m (Wang et al., 2017a).

3. Materials and methods

A total of 251 core samples, including 189 sandstone samples and 62 mudstone samples, were collected from 19 exploration wells in the Eocene Es4s beach-bar interval in the Boxing Sag (Fig. 1). Twenty-four samples were taken from 3168 m to 3175 m in Well F-137. In order to highlight pores, all the rock samples were impregnated with blue resin prior to sectioning. Carbonate minerals were distinguished in the thin sections through staining with Alizarin Red S and K-ferricyanide. Petrographic compositions of 189 samples were determined using point

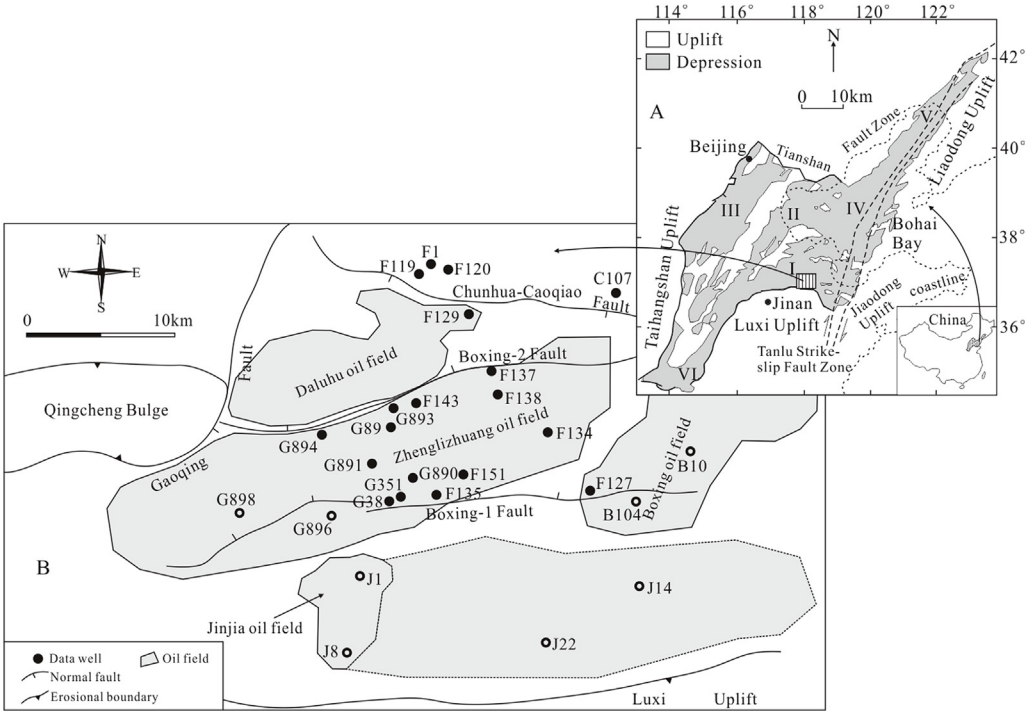

Fig. 1. (A) Tectonic setting of the Boxing Sag in the southern Jiyang subbasin (Sector I in (A)), Bohai Bay Basin. Other subbasins within the Bohai Bay Basin include the Huanghua subbasin (Sector II in (A)), Jizhong subbasin (Sector III in (A)), Linqing subbasin (Sector IV in (A)), Bozhong subbasin (Sector V in (A)) and Liaohe subbasin (Sector VI in (A)). (B) Structural map of the Boxing sag with the well locations and the main faults in the Es4s unit.

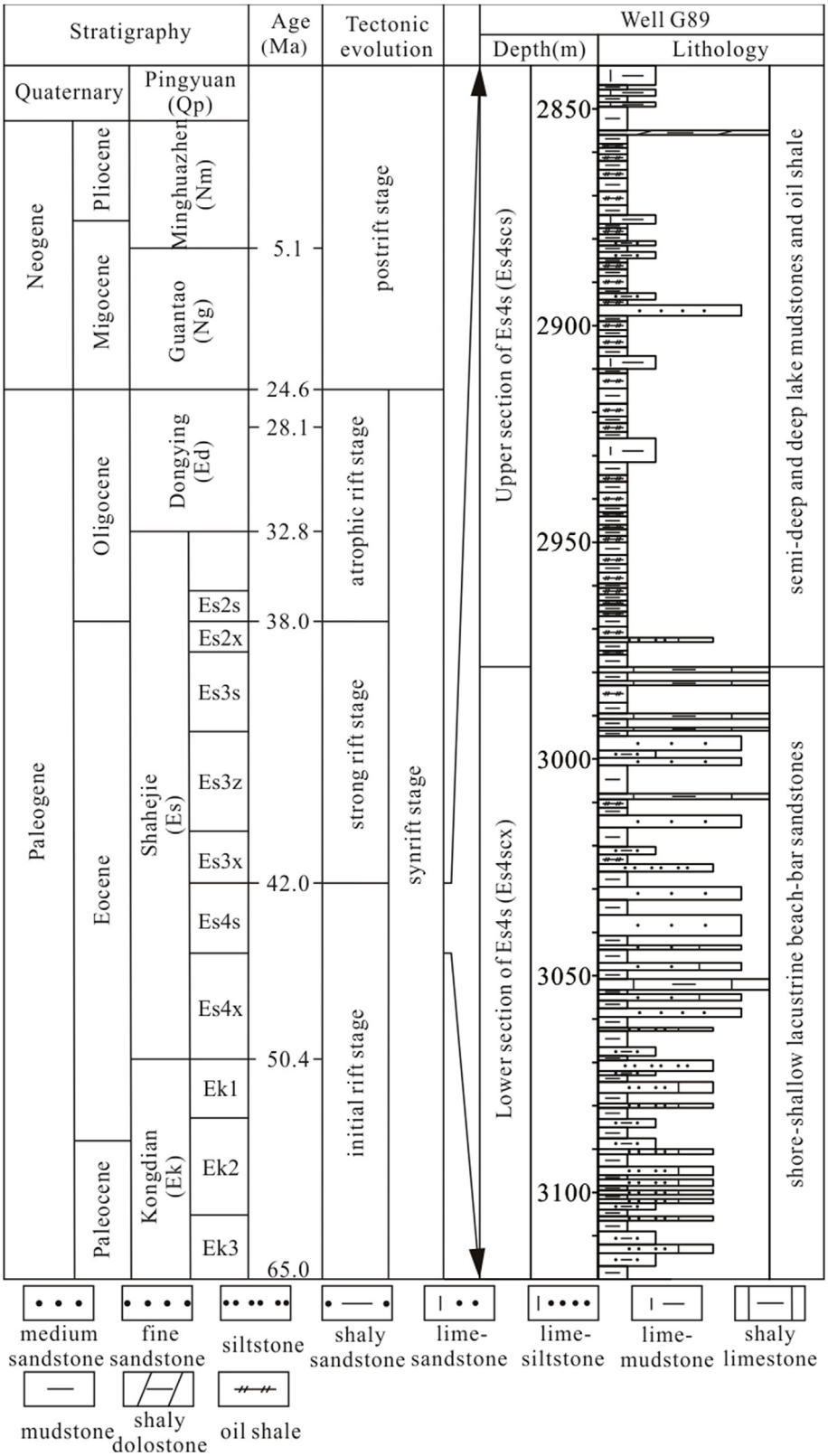

Fig. 2. Schematic Tertiary stratigraphy and tectonic evolution of the Boxing Sag. The Es4s unit developed during the initial rift stage and comprises sandstones that are interbedded with mudstones. Beach-bar sandstones mainly occur in the lower part of the Es4s Formation.

counting whereby counting total of 300 points were counted per thin section. The Udden-Wentworth grain size scale was used to determine the sandstone grain size (Udden, 1914; Wentworth, 1922). The sorting parameter was determined according to the standard charts of Folk (1980). Mineralogical compositions of mudstones were analyzed by X-ray diffraction (XRD) using a D8 DISCOVER with Cu-Ka radiation, a voltage of 40 kV, and a current of 25 mA. Before analysis, all samples were oven-dried at 40 °C for 2 days. In order to completely disperse the

minerals, an agate mortar was used to ground these samples to less than 40 mm without chemical pre-treatment. The samples were scanned from 3° to 70° with a step size of 0.02°. The relative content of the multiple mineral phases in weight percent was identified through XRD diffractograms and analyzed semiquantitative.

Based on thin section and SEM studies of the carbonate cement types and occurrence, samples with a high proportion of carbonate cement were selected to perform carbon and oxygen isotope analyses. Because the carbonate cements in this study were mainly composed of calcite, dolomite and ankerite, the particle size range was strictly controlled during the sample preparation to avoid interferences and cross contamination between the two mineral phases. The selected 108 rock samples were first ground below 200 mesh and then filtered through a 325 mesh sieve. After that the grains used for analysis were mostly approximately 5 μm − 44 μm CO_2 was extracted using the stepwise reaction method of Al-Aasm et al. (1990). The carbon and oxygen isotopes of CO_2 were analyzed using a Finnigan Mat 250 mass spectrometer. The Peedee belemnite (PDB) standard was used for the carbon isotope analysis, while the standard mean ocean water (SMOW) standard was used for the oxygen isotope analysis. The precisions of the carbon and oxygen isotope ratios were ± 0.2‰ and ± 0.3‰, respectively. The oxygen isotope ratios using the PDB standard were calculated using the equation $\delta^{18}O_{v\text{-}SMOW} = 1.03086 \times \delta^{18}O_{v\text{-}PDB} + 30.86$ of Friedman and O'Neil (1977).

One inch diameter standard cylindrical core plugs were used to measured porosity and permeability. The porosity was measured following Boyle's Law on the basis of helium porosimeter measurements. The pre-processed samples (dry, clean) were injected with helium at approximately 200 psi in a porosimeter. The grain volume was calculated through the Boyle's Law equation by measuring the corresponding pressure and volume. The bulk volume of the sample was measured using the Archimedes Principle with mercury immersion and was used to determine the pore volume by subtracting the grain volume. The grain volume and bulk volume were then used to calculate the total porosity.

4. Results

4.1. Lithology, grain order, and petrology of beach-bar sandstones

Core observation indicates the beach-bar deposits are characterized by frequently intervals of thin layers (usually 0.5–4.5 m) of sandstones and mudstones. The beach-bar deposits usually show the reverse graded sequence from argillaceous siltstone to siltstone and fine sandstone vertically (Fig. 3A and B). At the bottom of the sequence, there is no obvious interface between the mudstone and argillaceous siltstone but is often changed from mudstone to argillaceous siltstone gradually (Fig. 3A, D). At the top of the sequence, there is usually an abrupt interface between the fine sandstone and mudstone (Figs. 3A, C and 4). There is no obvious grain size change between the lower mudstone and the upper adjacent argillaceous siltstone, but the mudstone and argillaceous siltstone can be separated according to the median grain size and silt content at the depth of 3173.69 m (Figs. 3 A and 4). This kind of interface between mudstone and argillaceous siltstone is called gradual contact and the corresponding sandstone and mudstone are called the graded sandstone (G-sandstone) and graded mudstone (G-mudstone), respectively. There is an obvious grain size change at the depth of 3169.47 m in Well F-137, the interface between the fine sandstone and mudstone is called sharp contact (Figs. 3 A and 4), and the corresponding sandstone and mudstone are called sudden change sandstone (S-sandstone) and sudden change mudstone (S-mudstone), respectively.

The compositions of the Eocene beach-bar sandstones in the Dongying Depression were summarized By Wang et al. (2017a). The detrital compositions of beach-bar sandstones are mainly lithic arkoses according to Folk (1980) classification scheme, with corresponding average composition being $Q_{44.9}F_{34.9}R_{20.2}$ (Wang et al., 2017a). The interstitial materials of the beach-bar sandstones consist mainly of matrix (clay matrix and calcareous matrix) and cements (calcite, dolomite and ankerite with a minor amount of quartz overgrowths and clay minerals) (Wang et al., 2017a,b). Data from 3168 m to 3175 m in Well F-137 indicates that the compositions of beach-bar sandstones have good correlation with the depositional sequence. From bottom to up, the quartz content shows a gradually increasing trend, the K-feldspar and plagioclase contents firstly decrease and then increase, the rock fragment content show a gradually decreasing trend, clay matrix and calcareous matrix contents show gradually decreasing trends, and the carbonate cement contents also firstly decrease and then increase (Fig. 4). Carbonate cements mainly distribute in the bottom G-sandstone and top S-sandstone in a depositional sequence.

The compositions of S-sandstone and G-sandstone are shown in Table 1. The characteristics and detrital components of the G-sandstones are similar to that of the S-sandstones. Detrital quartz is the most abundant component. Detrital feldspars include both K-feldspar and plagioclase. Lithic fragments are mainly of volcanic and metamorphic in origins, with a small amounts of sedimentary fragment. Matrix mainly comprises clay matrix and calcareous matrix. Calcareous matrix in G-sandstone is higher than that in S-sandstone. Calcite cement content in S-sandstone is higher than that in G-sandstone, while the ankerite cement content is higher in G-sandstone.

4.2. Petrological characteristics of interbedded mudstones

Compared the XRD results of the S-mudstones and G-mudstones, the S-mudstone and the G-mudstone comprise similar component contents of detrital quartz, K-feldspar and plagioclase feldspar (Table 2). Calcite in the G-mudstones is more abundant than that in the S-mudstones. Dolomites in the S-mudstone and the G-mudstone are very low. Ankerite in the G-mudstone is much more abundant than that in the S-mudstone. The content of clay in the S-mudstone is higher than that in the G-mudstone. The TOC in the S-mudstone is more abundant than that in the G-mudstone (Table 2).

4.3. Characteristics of carbonate cements in beach-bar sandstones and mudstones

4.3.1. Microscopic characteristics of carbonate cements

Carbonate cements in the S-sandstones, G-sandstones, S-mudstone and G-mudstone mainly occur as calcite, dolomite and ankerite (Tables 1 and 2). The size and occurrences of calcite, dolomite and ankerite in beach-bar sandstones and corresponding mudstones are shown in Table 3. Calcite cements in S-sandstones fill almost all the intergranular pores, partly replacing detrital feldspar grains (Fig. 5A and B). Dolomites and ankerites in the S-sandstones mainly occur at the edge of calcite and tend to surround and replace calcites and detrital grains (Fig. 5A, B, F, and G). Microcrystalline (Fig. 5C) or micritic (Fig. 5D) calcites mainly occur in G-sandstone, which fill almost all the intergranular pores. Only a small amounts of the G-sandstones contain trace dolomites, whereas ankerites occur in almost every sample with varied amounts. Dolomites and ankerites in G-sandstones fill in intergranular pores, and surround and replace detrital grains (Fig. 5H and I). Calcites in the center of sandstones (far away from the contacts of mudstone-sandstone) mainly occur as isolated coarse-crystalline cements of usually less than 5 vol %, while dolomites mainly occur as rhombic coarse crystals with very low abundance (Fig. 5E). There is almost no occurrence of ankerites in the center of sandstones. Numerous intergranular and feldspar dissolution pores occur in the center of the sandstones (Fig. 5E). Carbonates in the S-mudstones and the G-mudstones distribute between grains and matrixes sporadically as patches with euhedral or subhedral crystals (Fig. 5J, K, L).

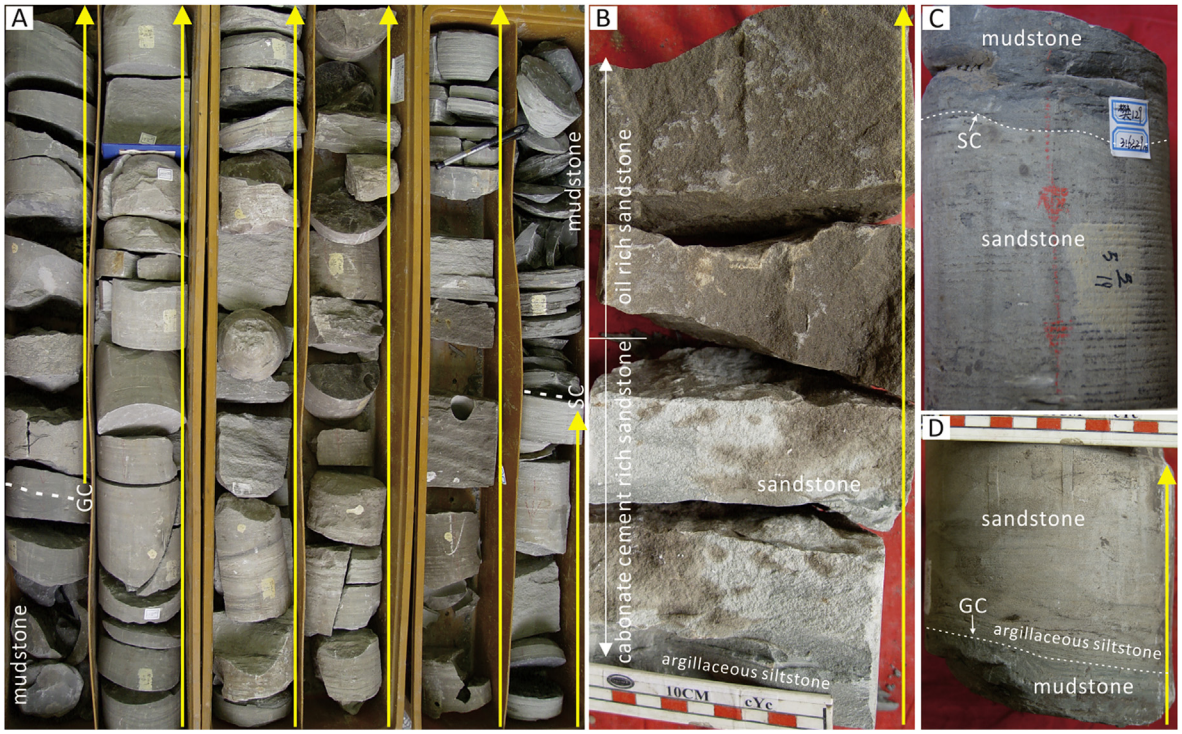

Fig. 3. Types and characteristics of sandstone-mudstone contacts and depositional sequence of the Eocene beach-bar intervals in the Boxing Sag. (A) Well F-137, 3169.1–3173.9 m, at the depth of 3173.69 m the gradual contact separates the mudstone and argillaceous siltstone; at the depth of 3169.47 m the sharp contact separates the mudstone and sandstone; the long yellow arrows show the reverse grain size order beach-bar sandstones from the depth of 3173.69 m to the depth of 3169.47 m. (B) Well G-351, 2444.69–2444.90 m, reverse grain size order beach-bar sandstones (long yellow arrow), the lower part is carbonate cement rich sandstone and the upper part is oil rich sandstone; (C) Well F-129, 3163.29 m, sharp contact between sandstone and mudstone; (D) Well F-137, 3165 m, reverse grain size order beach-bar mudstone-sandstones (long yellow arrow) with gradual contact. SC-sharp contact, GC-gradual contact. (For interpretation of the references to colour in this figure legend, the reader is referred to the Web version of this article.)

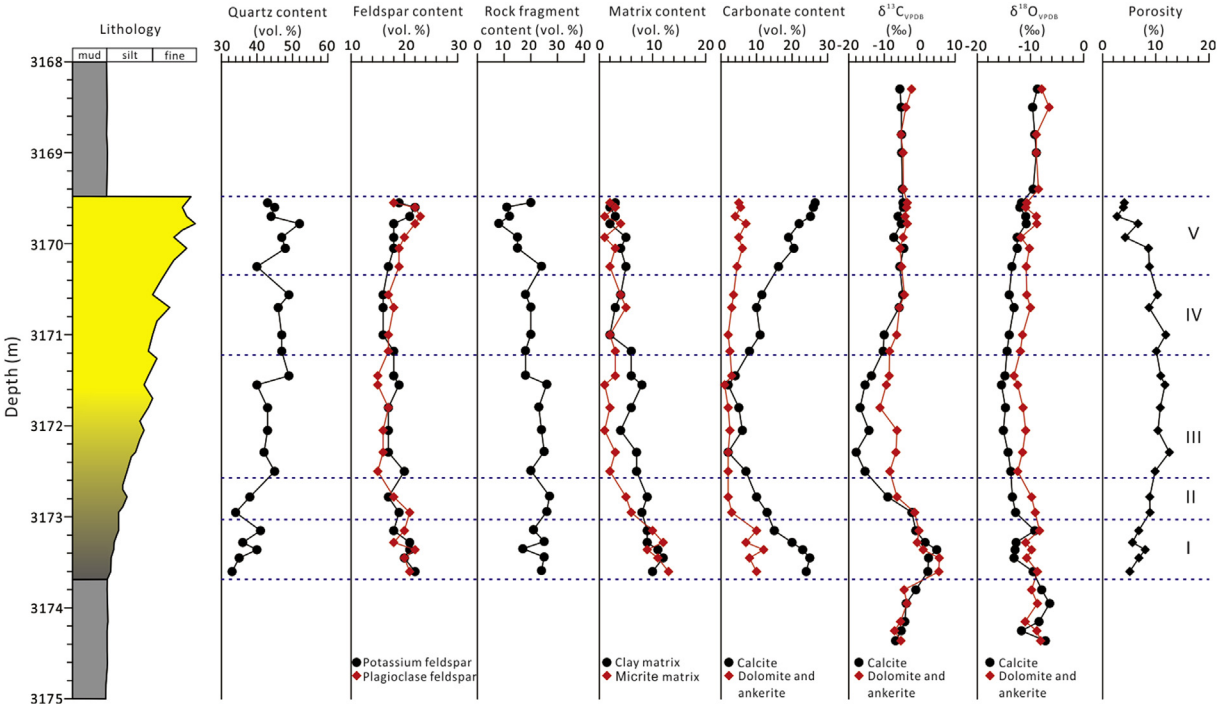

Fig. 4. Vertical profile of lithology, compositions, carbon and oxygen isotopes and porosity in a depositional sequence of beach-bar deposits in Well F-137 in the Boxing Sag.

Table 1
Modal composition of sandstone samples from the Eocene beach-bar intervals in the Boxing Sag.

	S-sandstone (n = 87)			G-sandstone (n = 64)		
	Min	Max	Mean	Min	Max	Mean
Lithic grains						
Quartz (vol. %)	25.4	53.5	40.9	24.1	52.3	39.5
Potassium feldspars (vol. %)	10.2	23.7	17	8.4	25.6	16.6
Plagioclase feldspars (vol. %)	14.8	23.4	17.7	8.8	30.2	16
Volcanic lithic fragments (vol. %)	1.3	37.2	12.7	1.6	45.7	15.2
Metamorphic lithic fragments (vol. %)	5.1	18.5	10.2	5.2	19.6	9.7
Sedimentary lithic fragments (vol. %)	0	6.2	1.5	0	16.7	2.8
Mica (vol. %)	0	0.5	0.1	0	2.5	0.1
Chert (vol. %)	0	2	0.2	0	2.3	0.2
Clay matrix (vol. %)	0	9.3	4.9	1.2	12.3	5.9
Calcareous matrix (vol. %)	0	5.7	1.1	3.7	15.3	7.8
Diagenetic alteration						
Calcite (vol. %)	12.4	27.2	20.1	6	24.3	15.6
Dolomite (vol. %)	0	7.4	1.4	0	3.3	1.6
Ankerite (vol. %)	1.2	5.4	2.6	0	25.3	5.3
Clay minerals (%)	0	9.9	4.9	1.2	12.3	5.9
Kaolinite (%)	1	36	22.3	2	38	24.3
Illite (%)	25	71	44.9	29	67	41.1
Illite-smectite mixed layers (%)	4	49	25.6	3	53	27.8
Chlorite (%)	1	20	7.2	1	18	6.8
Pyrite (vol. %)	0	5.6	0.3	0	2.6	0.2

Table 2
Modal composition of mudstone samples from the Eocene beach-bar intervals in the Boxing Sag.

	S-mudstone (n = 32)			G-mudstone (n = 20)		
	Min	Max	Mean	Min	Max	Mean
Quartz (wt. %)	20	31	27.9	20	33	27.6
Potassium feldspars (wt. %)	0	7	4.1	3	15	6.4
Plagioclase feldspars (wt. %)	8	19	13.8	8	21	14.4
Calcite (wt. %)	7	15	10.1	13	16	15.2
Dolomite (wt. %)	0	4	2.6	0	2	0.8
Ankerite (wt. %)	0	3	0.6	0	20	9.6
Clay (wt. %)	30	53	39.9	11	34	24.8
Kaolinite (wt. %)	1	9	3.8	0	8	3.8
Illite-smectite mixed layers (wt. %)	34	80	54.5	33	76	56.8
Illite (wt. %)	17	58	36	16	65	30.6
Chlorite (wt. %)	3	16	4.8	2	12	5.8
Ratio of illite-smectite mixed layers	20	45	25	20	40	25
Pyrite (wt. %)	0	3	1	0	2	1.2
TOC (wt. %)	1.2	3.1	2.3	0.9	2	1.3

4.3.2. Distribution characteristics of carbonate cements in beach-bar sandstones

The carbonate cement content has no correlation with the matrix content in the S-sandstone, while the carbonate cement content has a positive relationship with the matrix content in the G-sandstone (Fig. 6). Carbonate cement content decreases gradually from the sharp contact to the center of sandstone in different depth ranges (Fig. 7A). Carbonate cement content also shows decreasing characteristics from the gradual contact to the center of sandstone, but low carbonate cement content still occurs in the G-sandstone (Fig. 7B). Detail carbonate cement content and porosity analysis in a depositional sequence from 3168 m to 3175 m in Well F-137 indicates that the carbonate cement

Table 3
Characteristics of carbonates and grain contacts of the Eocene beach-bar sandstones and mudstones in the Boxing Sag.

		S-sandstone	G-sandstone	Center part of sandstone	S-mudstone	G-mudstone
Calcite	Size	Up to 250 μm	< 10 μm	Up to 200 μm	< 5 μm	< 20 μm
	Occurrence	Coarse-crystalline calcites (blocky crystals)	Microcrystalline or micritic calcites, comprising patch-like cements	Isolated coarse-crystalline calcites	Microcrystalline cements as patches with euhedral or subhedral crystals	Microcrystalline cements as patches with euhedral or subhedral crystals
	$\delta^{13}C_{VPDB}$	−10.3‰ to −2.5‰	−2.2‰–4.8‰	−17.9‰ to −4.8‰	−5.6‰ to −0.2‰	−6.8‰–0.4‰
	$\delta^{18}O_{VPDB}$	−13.5‰ to −10.4‰	−14.3‰ to −9.2‰	−15.5‰ to −13‰	−12.1‰ to −6.9‰	−13.7‰ to −6.4‰
Dolomite and ankerite	Size	< 50 μm	< 5 μm	< 100 μm	< 10 μm	< 10 μm
	Occurrence	Mainly occur at the edge of calcite and tend to surround and replace calcites and detrital grains	Rhombic microcrystals, comprising the blocky assemblages	Isolated coarse-crystalline dolomites	Microcrystalline cements as patches with euhedral or subhedral crystals	Patch-like aggregates with relatively complete crystal form
	$\delta^{13}C_{VPDB}$	−5.5‰–0.3‰	−0.4‰–5.5‰	−11.2‰ to −3.2‰	−5.3‰ to −0.8‰	−7.1‰–1‰
	$\delta^{18}O_{VPDB}$	−11.9‰ to −7.6‰	−10.7‰ to −3.8‰	−13.1‰ to-8.6‰	−8.9‰ to −6.4‰	−11‰ to −5.7‰
Grain contact		Point contact or point-line contact	Mainly point contacts with minor amounts of point-line contacts	Mainly point-line contact		

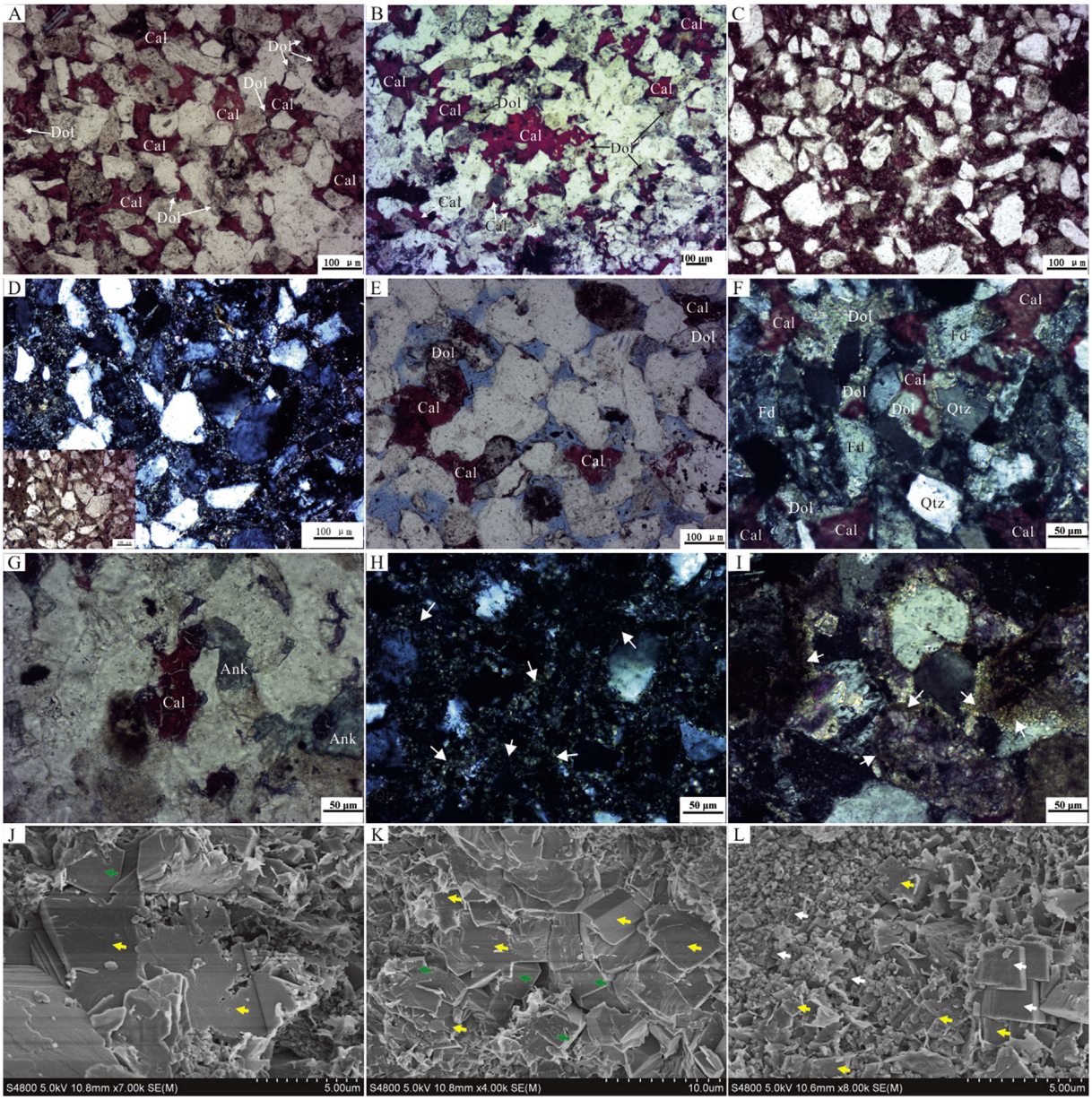

Fig. 5. Occurrence of carbonate cements (calcite and dolomite) at the edge of the S-sandstones and G-sandstones of Eocene beach-bar in the Boxing Sag. (A) Well G-351, 2455.14 m, S-sandstone, coarse-crystalline calcites and minor amounts of dolomites filling in intergranular pores and replacing detrital grains, and dolomites mainly occur at the edge of calcites (polarized light). (B) Well G-38, 2403.7 m, S-sandstone, coarse-crystalline calcites and minor amounts of dolomites filling in intergranular pores and replacing detrital grains with dolomites mainly occurring at the edge of calcites (polarized light). (C) Well G-890, 2612.4 m, G-sandstone, microcrystalline calcites filling in intergranular pores and replacing detrital grains (polarized light). (D) Well F-135, 2531.55 m, micritic calcites with re-crystallization filling in intergranular pores and replacing detrital grains (crossed polarizers, small photo is under polarized light). (E) Well G-890, 2598.2 m, center part of sandstone, isolated coarse crystalline calcites and dolomites filling in intergranular pores (polarized light). (F) Well F-129, 3163.39 m, S-sandstone, dolomites filled in intergranular pores surround and replaced calcites (crossed polarizers). (G) Well F-120, 3323.8 m, S-sandstone, ankerites filled in intergranular pores and replaced calcites and grains (polarized light). (H) Well F-120, 3322 m, G-sandstone, microcrystalline ankerites filling in intergranular pores and replacing detrital grains (crossed polarizers). (I) Well G-351, 2428.04 m, G-sandstone, microcrystalline ankerites with recrystallization filling in intergranular pores and replacing detrital grains (crossed polarizers). (J) Well F-151, 2729.2 m, microcrystalline calcites (yellow arrows) and dolomites (green arrows) with relatively complete crystallographic form in the S-mudstone. (K) Well F-129, 3164.3 m, patches of microcrystalline calcites (yellow arrows) and dolomites (ankerites) (green arrows) with euhedral or subhedral crystals in the S-mudstone. (L) Well F-151, 2728.3 m, patches of microcrystalline calcites (yellow arrows) and ankerites (white arrows) with relatively complete crystallographic forms in the G-mudstone. (For interpretation of the references to colour in this figure legend, the reader is referred to the Web version of this article.)

content can be divided into five zones from bottom to top (Fig. 4). The zone I is characterized by high content of microcrystalline carbonate cement (av. 20.7% calcite and av. 7.9% dolomite and ankerite) and low porosity (av. 8%). The carbonate cements in the zone II (av. 9% calcite and av. 3.1% dolomite and ankerite) mainly occur as microcrystalline calcite, dolomite and ankerite and isolated crystalline calcite and dolomite. The average porosity of the zone II is 11.7%. The zone III is characterized by lowest content of coarse isolated crystalline calcite and dolomite (av. 4.5% calcite and av. 1.9% dolomite) and highest porosity (13.1%). The carbonate cements in zone IV mainly occur as coarse isolated crystalline calcite (av. 9.9%) and dolomite and ankerite (av. 2.5%) and the average porosity is 9.7%. High content of coarse

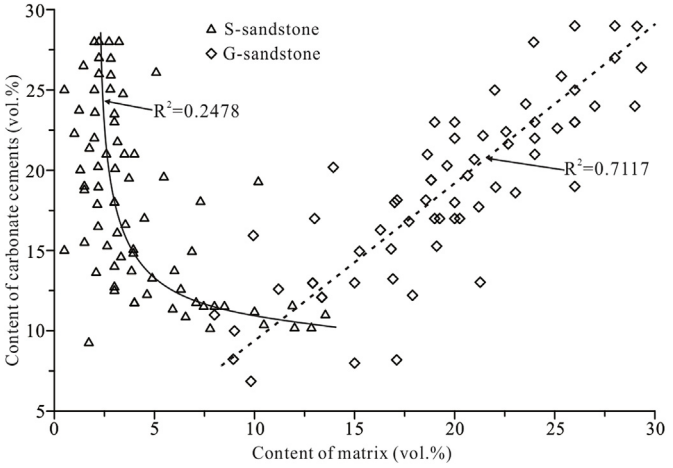

Fig. 6. Correlations between carbonate cement contents and matrix contents in the S-sandstone and G-sandstone of the Eocene beach-bar intervals in the Boxing Sag.

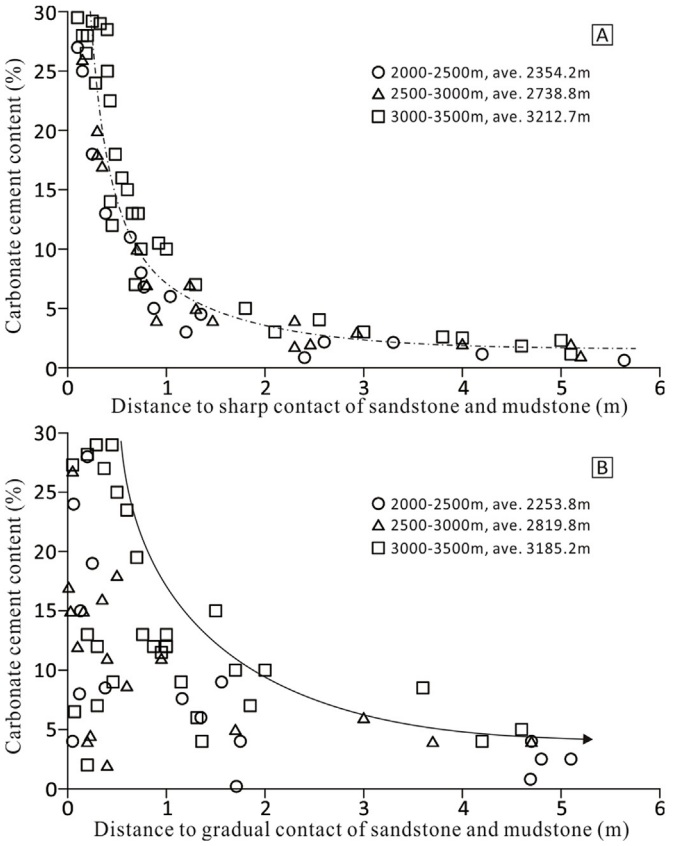

Fig. 7. Carbonate cement contents in the S-sandstone and G-sandstone from the contact to the center of sandstones of the Eocene beach-bar intervals in the Boxing Sag.

crystalline calcite (av.22.5%) and dolomite (av. 5%) mainly occur in zone V and the average porosity is very low (5.8%).

4.3.3. Carbon and oxygen isotopic compositions of carbonate cements

The characteristics and distribution of bulk carbon and oxygen isotope ratios of calcites and dolomites and ankerites in sandstone and mudstone are shown in Table 3 and Fig. 8. Calcite and dolomite in the middle part of the sandstone have the lightest carbon and oxygen isotopic compositions (Table 3 and Fig. 8). The $\delta^{13}C$ of calcite and dolomite and ankerite in S-sandstones is lighter than that in G-sandstones (Table 3 and Fig. 8). The $\delta^{18}O$ of calcite in S-sandstone and G-sandstone is almost in the same range, which is lighter than that of dolomite and ankerite in S-sandstone and G-sandstone (Table 3 and Fig. 8). The $\delta^{13}C$ and $\delta^{18}O$ of calcite and dolomite and ankerite in S-mudstone and G-mudstone is almost in the same range (Table 3 and Fig. 8). From the sharp contact to the center of sandstone the $\delta^{13}C$ and $\delta^{18}O$ of calcite and dolomite and ankerite become lighter gradually (Fig. 9A and B). The $\delta^{13}C$ and $\delta^{18}O$ of calcite and dolomite and ankerite also have the gradually lighter characteristics from the gradual contact to the center of sandstone (Fig. 9C and D). Detail analysis of carbon and oxygen isotopic compositions of carbonate cements in a depositional sequence from 3168 m to 3175 m in Well F-137 indicates that the $\delta^{13}C$ and $\delta^{18}O$ of calcite and dolomite and ankerite in S-mudstone and G-mudstone have no significance difference (Fig. 4). The $\delta^{13}C$ of calcite and dolomite and ankerite in G-sandstone (Zone I) is heavier than that of calcite and dolomite and ankerite in S-sandstone (Zone V), while the $\delta^{18}O$ of calcite and dolomite and ankerite in G-sandstone and S-sandstone are in the same range (Fig. 4). There is no significance difference of the $\delta^{13}C$ and $\delta^{18}O$ of calcite and dolomite and ankerite between the transition zone II and transition zone IV (Fig. 4). The calcite and dolomite in the central part of sandstone (Zone III) have the lightest carbon and oxygen isotopic compositions (Fig. 4).

5. Discussion

5.1. Precipitation temperatures of carbonate cements in sandstones and mudstones

Using the $\delta^{18}O_{VPDB}$ values of the calcite cements in sandstones and mudstones, the fractionation equation of Friedman and O'Neil (1977), and assuming that the $\delta^{18}O_{V\text{-}SMOW}$ values for the pore water is −2‰ to 0‰, which are common for evolved formation water in the early-moderate burial stage of the Eocene Dongying depression because of the arid-semi-arid climate and high salinity sedimentary water (Wang et al., 2016, 2017b), the precipitation temperatures of the calcite cements in sandstones and mudstones were calculated (Fig. 10A, C). In order to comparatively analyze the differences of the precipitation temperatures of calcite cements, three analytical ranges were divided from the boundary to the center of sandstones according to the content and distribution of carbonate cements in sandstones, which are less than 0.5 m to the sharp contact, 0.5–1 m to the sharp contact and more than 1 m to the sharp contact, respectively. The precipitation temperatures of calcite cements in the three analytical ranges from the sharp contact to the center of sandstones are in the ranges of 62°C–99.4 °C (av. 83.5 °C), 65.5°C-115.5 °C (av. 88.4 °C) and 84.7°C-121 °C (av. 100.8 °C), respectively (Fig. 10A). From the sharp contact to the center of sandstones the precipitation temperatures of calcite cements increase gradually, which means that the precipitation temperatures of coarse-crystalline calcites in the S-sandstones are lower than that of the isolated coarse-crystalline calcites in the center of sandstones. The precipitation temperatures of calcite cements in the three analytical ranges from the gradual contact to the center of sandstones are in the ranges of 54.1°C–111.3 °C (av. 85.2 °C), 54.1°C-113.4 °C (av. 87.8 °C) and 87.2 °C −124.4 °C (av. 105.3 °C), respectively (Fig. 10C), which also show the increasing characteristics from the boundary to the center of sandstones. The precipitation temperatures of calcite cements in the S-sandstones and G-sandstones have no significance differences, but the temperature gradient in the S-sandstone far from the sharp contact is greater than that in the G-sandstone far from the gradual contact. The precipitation temperatures of calcites in the S-mudstones and G-mudstones are in the ranges of 40.4°C–90.3 °C (av. 62.9 °C) and 37.6°C-105.2 °C (av. 59 °C), respectively (Fig. 10A, C), which are lower than that of calcite cements in the adjacent S-sandstones and G-sandstones.

Using the fractionation equation of Land (1983), and assuming that the $\delta^{18}O_{V\text{-}SMOW}$ values are −1‰ to 1‰ for the pore water, which is

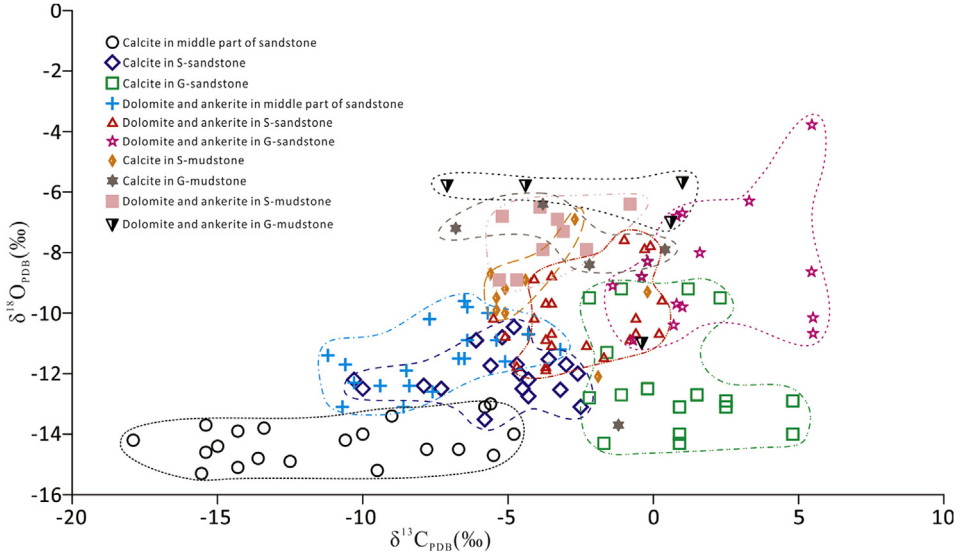

Fig. 8. Cross plots showing the distributions and correlations of $\delta^{13}C_{PDB}$ and $\delta^{18}O_{PDB}$ of calcite and dolomite and ankerite in sandstones and mudstones of the Eocene beach-bar intervals in the Boxing Sag.

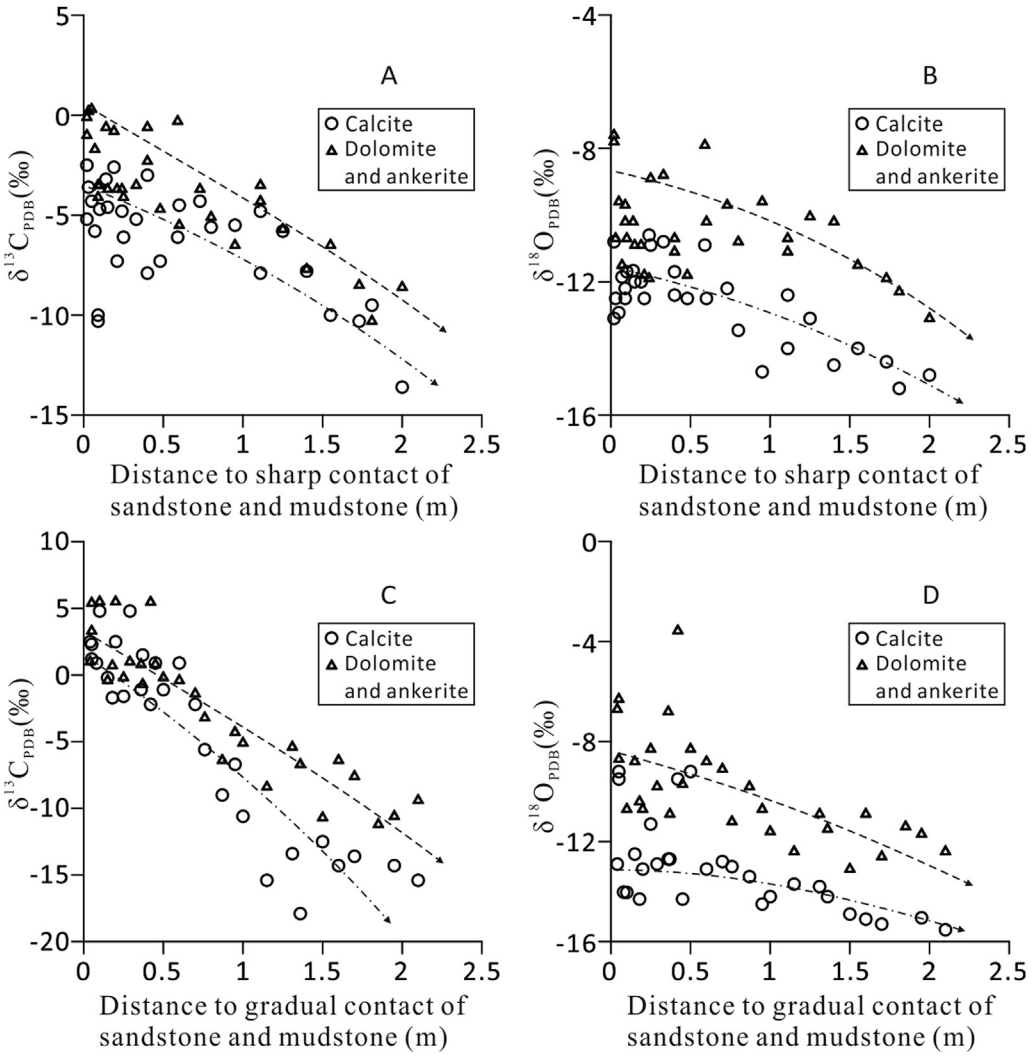

Fig. 9. Distribution of $\delta^{13}C_{PDB}$ and $\delta^{18}O_{PDB}$ of calcite and dolomite and ankerite from the contact to the center of sandstones of the Eocene beach-bar intervals in the Boxing Sag.

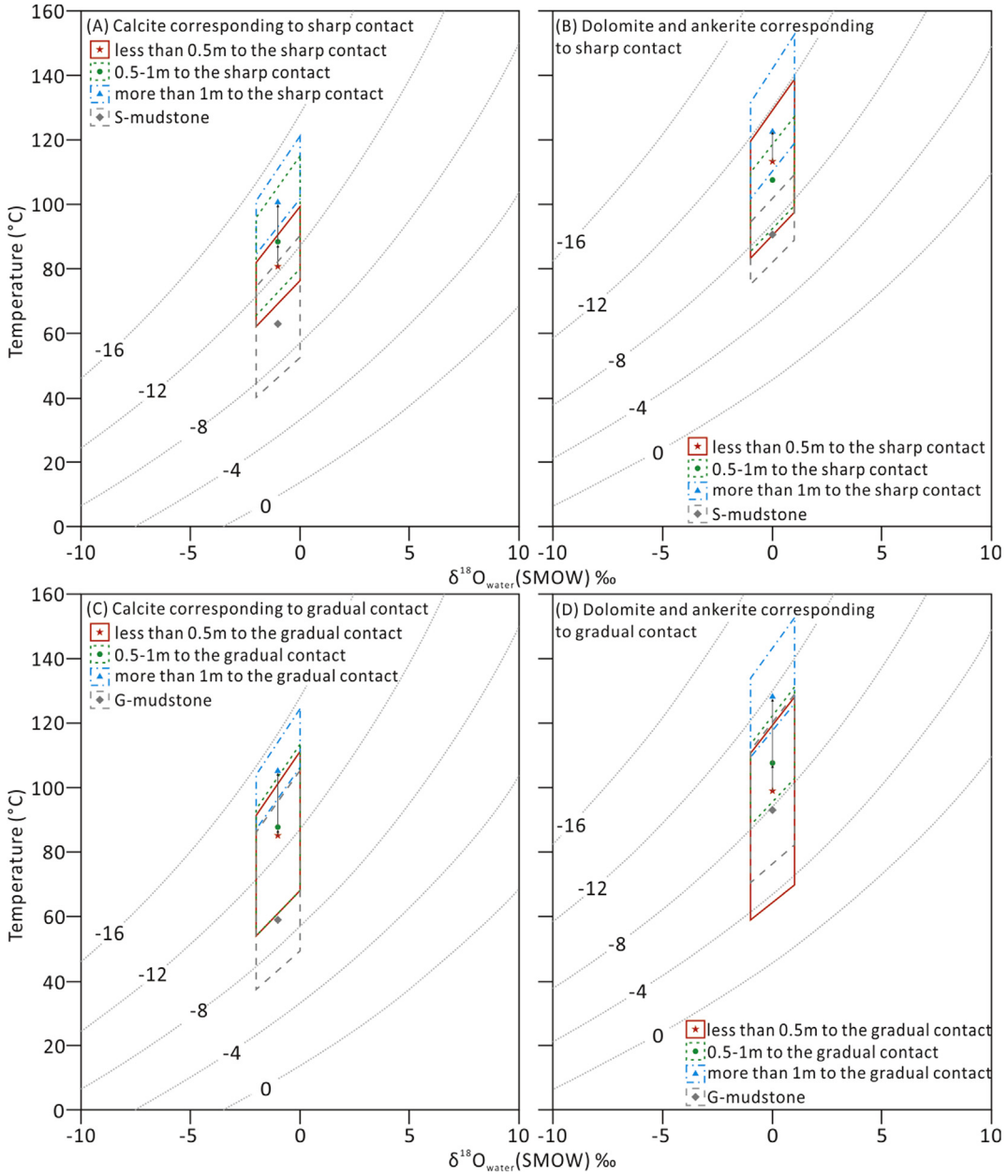

Fig. 10. Diagrams showing the range of temperatures calculated from the assumed oxygen isotopic composition of the pore water and $\delta^{18}O$ values of: (A) Calcite corresponding to the sharp contact between S-sandstone and S-mudstone using the fractionation equation of Friedman and O'Neil (1977), (B) Dolomite and ankerite corresponding to the sharp contact between S-sandstone and S-mudstone using the fractionation equation of Land (1983), (C) Calcite corresponding to the gradual contact between G-sandstone and G-mudstone using the fractionation equation of Friedman and O'Neil (1977), and (D) Dolomite and ankerite corresponding to the gradual contact between G-sandstone and G-mudstone using the fractionation equation of Land (1983).

equivalent to moderately to highly evolved formation waters relative to the contemporary Eocene $\delta^{18}O_{V\text{-}SMOW}$ value of lake water (Wang et al., 2016, 2017b), the precipitation of dolomite and ankerite cements in sandstones and mudstones were calculated (Fig. 10B, D). The precipitation temperatures of dolomite and ankerite cements in the three analytical ranges from the sharp contact to the center of sandstones are in the ranges of 83.3°C–138.8 °C (av. 113.4 °C), 85.4°C-127.1 °C (av. 107.6 °C) and 101.7°C-152.7 °C (av. 122.7 °C), respectively (Fig. 10B), while the precipitation temperatures of dolomite and ankerite cements from the gradual contact to the center of sandstones are in the ranges of 59°C–128.2 °C (av. 99.1 °C), 88.4°C-131.2 °C (av. 107.7 °C) and 109.5°C-152.7 °C (av. 128.4 °C), respectively (Fig. 10D). The precipitation temperatures of dolomite and ankerite in the -sandstone and G-sandstone have no significance difference, but both of them are lower than that from the center of sandstones. The precipitation temperatures of dolomite and ankerite cements in the S-mudstones and G-mudstones are in the ranges of 75°C–109.2 °C (av. 90.6 °C) and 70.5°C-129.2 °C (av. 93.1 °C), respectively (Fig. 10B, D), which are lower than that in the adjacent S-sandstones and G-sandstones. The precipitation temperatures of dolomite and ankerite cements are higher than that of calcite cements in the same analytical range to interface (Fig. 10).

5.2. Material sources of carbonate cements in sandstones

5.2.1. Material source of carbonate cements in S-sandstones

The sources for the carbonate cements in the clastic reservoirs are either internal or external (Dutton, 2008). The amount of carbonate rock fragments in the S-sandstone is very low and is insufficient to serve

as the source for the carbonate cements. The content of carbonate cements has no correlation with matrix content also indicate that the carbonate cements in the S-sandstone are most likely sourced externally. Due to the aforementioned distribution characteristics, carbonate cement content decreases gradually from the sharp contact to the center of the sandstone (Figs. 4 and 7A), indicating that these cements in the S-sandstones are external and are most likely related to the diagenesis of the interbedding mudstones (Milliken and Land, 1993; Wang et al., 2016, 2018). During the Eocene beach-bar deposition in the Boxing Sag, the salinity of the deposition water was likely high due to the enclosed nature of the lake during prolonged droughts (Wang et al., 2017b), which resulted in high contents of calcareous components in the mudstones (Table 2). The relatively light carbon and oxygen isotopic compositions (Figs. 4 and 8) and relatively high precipitation temperatures of calcites and dolomites and ankerites in the S-mudstones (Fig. 10A and B) indicate that the calcareous components had experienced diagenetic alterations to some extent. A series of diagenetic alterations of clay minerals in the mudstones occurred with increasing burial, with the most important alteration being the conversion of smectite to illite (or chlorite). The reactions between K-feldspar and organic acids in the S-mudstones would have generated a large amount of kaolinite and Al^{3+} and K^{+}, supplying the necessary cations for the conversion of smectite to illite (or chlorite) (Macaulay et al., 1993). In the study area, the vertical change of clay minerals in mudstone indicates that kaolinite and smectite transformed to illite and chlorite during the burial process (Wang et al., 2017b). During the conversion process of smectite to illite, it would have released massive interlayer water and cations, such as Na^{+}, Ca^{2+}, Mg^{2+}, Fe^{2+} and Si^{4+} (Boles and Franks, 1979; McHargue and Price, 1982; Wang et al., 2018). The calcium ions in the calcareous component and the released ions provided necessary materials for the precipitation of carbonate cements at the boundary of the S-sandstones (Fig. 11). The released Mg^{2+} would have raised the ratio of Mg/Ca, together with the increased Fe^{2+}, which provided the material source for the formation of dolomites and ankerites within the S-sandstones (Fig. 11).

The stable carbon isotope ratios (Table 3 and Fig. 8) indicate that the calcite and dolomite and ankerite cements in the S-sandstone were influenced by organic CO_2 to some extent during the precipitation process (Sensula et al., 2006; Wang et al., 2016). The organic materials in the S-mudstones display a relatively high abundance. The precipitation temperatures of calcites, dolomites and ankerites in the S-sandstone are in the range of low mature and mature stages for organic materials, which would have generated a large amount of organic acids and CO_2. The participation of organic-origin CO_2 in the precipitation process would lead to light carbon isotope ratios of the calcites (Sensula et al., 2006).

5.2.2. Material source of carbonate cements in G-sandstones

Compared with the carbonate cements in the S-sandstones, the occurrences and the carbon isotope ratios of calcites and dolomites and ankerites in the G-sandstones indicate different carbonate material sources. The carbon isotope ratios of the microcrystalline calcite and dolomite and ankerite in G-mudstones (Table 3, Figs. 4 and 8), indicating the participation of organic CO_2 during the diagenetic alteration of carbonates in G-mudstones. The carbon isotope ratios of the microcrystalline carbonate cements in the G-sandstones (Table 3, Figs. 4 and 8) are in the range of carbon isotope ratios of lacustrine limestone (Kelts and Talbot, 1990), which is heavier than that of microcrystalline calcite in G-mudstone (Table 3, Figs. 4 and 8), indicating that the diagenesis and diagenetic products in the G-mudstones have little or no influence on the diagenesis of carbonate cements in the adjacent G-sandstones, which further explain the internal source for the carbonate cements in G-sandstone (Fig. 11).

Though the carbon isotope ratios of the microcrystalline carbonate cements in the G-sandstone are in the range of carbon isotope ratios of lacustrine limestone (Kelts and Talbot, 1990), the precipitation temperatures of the microcrystalline calcites and dolomites and ankerites in the G-sandstones are similar to that in S-sandstones, indicating that the microcrystalline carbonate cements in G-sandstone experienced diagenetic alterations. The occurrence of carbonates, distribution of carbonates from the gradual contact to the center of sandstone and the positive relationship between carbonate cement content and matrix content (Fig.5, Figs. 6 and 7B), indicating that the origin of the carbonate cements in the G-sandstone is most likely to be precipitated in situ by the diagenetic alterations of the high content of calcareous and clay matrix (Table 1).

5.2.3. Material source of carbonate cements in the center of sandstones

Compared with the carbonate cements in S-sandstones and G-sandstones, the carbonate cements in the center part of sandstones are characterized by low content, isolated coarse-crystals filling in primary and feldspar dissolution pores and lighter carbon and oxygen isotopic compositions (Table 3 and Figs. 7 and 8). The $\delta^{13}C$ of calcite and dolomite in the center part of sandstones indicate that the organic CO_2 were involved in the precipitation process, and the participation degree of organic CO_2 is getting gradually higher from the interface to the center of sandstones (Fig. 9A, C). The precipitation temperatures of calcite and dolomite in the center part of sandstones are significantly higher than that in S-mudstones and G-sandstones, which are in the most active temperature range of organic materials to generate organic CO_2 and acid (Surdam et al., 1989, 1993). The K-feldspar and plagioclase contents in the center part of sandstones are obviously lower than that in S-sandstones and G-sandstones (Fig. 4), and the content of feldspar dissolution pores in the center part of sandstones is obviously lower than that in S-sandstones and G-sandstones (Wang et al., 2017a), indicating that the carbonate cements precipitation and feldspar dissolution are genetically correlated (Fig. 4). Influenced by the injection of organic CO_2 and acid, a large number of feldspar in the center part of the sandstones were dissolved, providing massive Ca^{2+} for the precipitation of carbonate cements (Macaulay et al., 1993). Another important diagenetic products of feldspar dissolution is authigenic kaolinites that fills pores and distributes widely in the beach-bar sandstones (Wang et al., 2017a,b). The precipitation temperature of carbonate cements in the center part of sandstones (Fig. 10) is the optimal conversion range for clay minerals (Macaulay et al., 1993; Merriman, 2005). The conversion of kaolinite and smectite to illite released a large amount of Ca^{2+}, Mg^{2+}, Fe^{2+} ions, providing important materials for the precipitation of the carbonate cements. This phenomenon is consistent with clay minerals dominated by illites and illite-smectite mixed layers in the beach-bar sandstone reservoirs (Wang et al., 2017b).

The increasing content of feldspar and progressively heavier carbon and oxygen isotope ratios from the center to the boundary of the sandstones indicates that the influence degree of materials for carbonate cements precipitation from feldspar dissolution and organic CO_2 decrease gradually. There is usually a transition zone between the S-sandstone (G-sandstone) and the center part of the sandstone, take the Well F-137 (3168 m–3175 m) for example, the zone II and zone IV are the two transition zones with medium content of carbonate cements and medium carbon isotope ratios (Fig. 4).

5.3. Mass transfer from mudstone to sandstone during diagenesis

The occurrence and the material sources of carbonate cements in the S-sandstone and G-sandstone suggest that the mass transfer of carbonate cements was constrained by the property of sandstone-mudstone contact and mainly appeared in couples of S-mudstone and S-sandstone during diagenetic process.

Compaction flow and diffusion are the two mainly patterns of mass transfer between the mudstone and sandstone interbeds (Thyne, 2001; Dutton, 2008; Bjørlykke, 1993, 1994; Bjørlykke and Jahren, 2012). For the G-mudstone and G-sandstone couples, the matrix content at the boundary of sandstone is high, the grain size is fine, and the sorting is

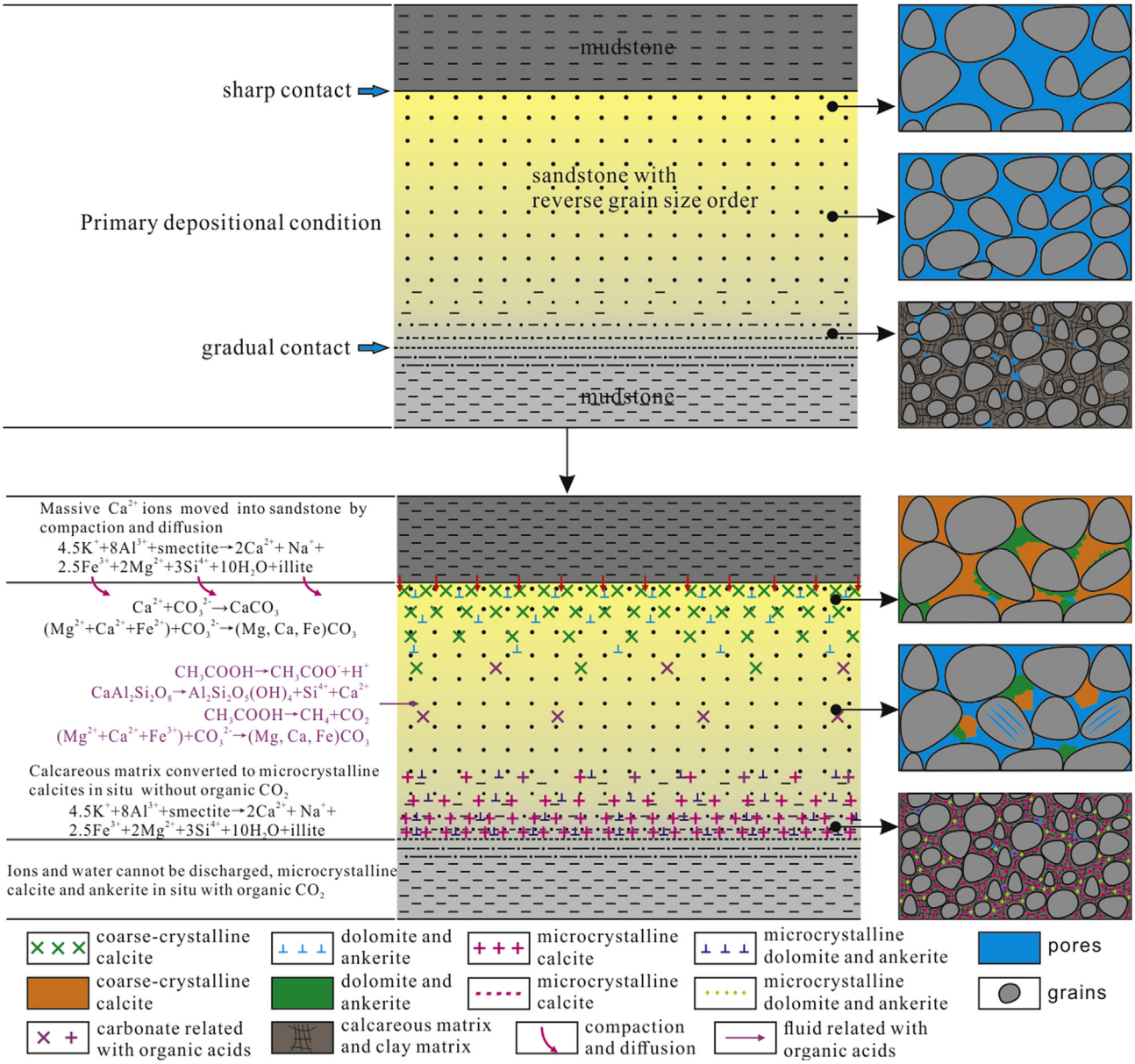

Fig. 11. Material sources and distribution of carbonate cements in the Eocene beach-bar sandstone and mudstone intervals in the Boxing Sag.

poor, causing the intergranular pores decrease rapidly during the shallow burial stage (Rossi et al., 2002; Dutton and Loucks, 2010; Rossi and Alaminos, 2014). High content of matrix contains diverse minerals and adsorbs a large number of calcium ions, which causes the ion concentration gradient to be very small between the G-mudstone and the G-sandstone. Extremely low diffusion coefficient at the boundaries of G-sandstones and the small concentration gradient cannot match the conditions of diffusion (Bjørlykke and Jahren, 2012). At this condition, the adsorbed and generated cations and fluids cannot be moved out from the G-mudstones but concentrated and took part in the in situ diagenesis (Fig. 11). The contents of calcite and ankerite in G-mudstones are significantly higher than that in S-mudstones (Table 2), also indicating that the mass in G-mudstones didn't move out during the burial process. Fluids and materials in the G-mudstones cannot produce effective effects on the diagenesis of the G-sandstones (Fig. 11). With increasing burial and temperature, calcareous matrixes in the G-mudstones and G-sandstones change into microcrystalline calcites through diagenetic alterations (Wenzel, 2000; Rott and Qing, 2013) (Fig. 5C and D). As the temperature continues to rise during the subsequent burial process, the conversion of smectite to illite releases massive Ca^{2+}, Mg^{2+}, Fe^{2+} ions and waters, which improves the ratio of Mg/Ca and is favorable for the formation of dolomite and ankerite (Fig. 5C and D).

Compared to G-sandstone, coarse grain size and low content of matrix can prevent compaction and retain a certain amount of intergranular pores in S-sandstone at shallow-medium burial depth (Dutton and Loucks, 2010). The petrographic characteristics and the relatively low precipitation temperatures indicate that the coarse-crystalline calcites in the S-sandstones were mainly precipitated during the burial stage when sediments have experienced weak-medium compaction and massive intergranular pores developed in the S-sandstones. Due to the pore waters discharged by compaction and the increasing temperature (Bjørlykke, 1993, 1994; 1996; Thyne, 2001), the ion concentration in the S-mudstones would increase gradually and form a concentration gradient through the S-mudstone-S-sandstone contact (Thyne, 2001; Bjørlykke and Jahren, 2012). With the increasing burial depth and temperature, organic acid and CO_2 may improve the solubility of carbonates to increase the fluid ion concentration (Barth and Bjørlykke, 1993; Wang et al., 2016). Meanwhile, the cations generated from the

conversion of clay minerals also increase the fluid ion concentration (Bjørlykke and Aagaard, 1992). The concentration gradient between the S-mudstones and the S-sandstones, and the high diffusion coefficient of the porous sandstones (Bjørlykke and Jahren, 2012) at the edges of the S-sandstones are conducive for diffusion. Diffusion causes massive metal ions and CO_2 transfer from the S-mudstone to the adjacent intergranular pore-developing S-sandstones. Compared to the silicate minerals, carbonates have the fast kinetic reaction rate, causing fast dissolution and precipitation of carbonates (Bjørlykke and Jahren, 2012), which is beneficial to the diffusion transportation from the S-mudstone to the S-sandstone. During this transportation from the S-mudstones to the S-sandstones, the initial chemical balance was disturbed by water-rock interactions within the new chemical environment, allowing carbonate cements to form along the boundaries of the sandstones (Dutton, 2008; Chen et al., 2009; Day-Stirrat et al., 2010; Dutton and Loucks, 2010). Such mass transfer via diffusion is hard to happen over a long distance (Bjørlykke and Jahren, 2012), thus the carbonate cements mainly distribute at the boundaries of sandstones (Fig. 4, Fig. 5A and B, and 7A, Fig. 11). From the contact to the center of the sandstone the content of carbonate cements decreases sharply because of the fast descending fluid concentration in the S-sandstone. A greater conversion depth of the clay minerals in the mudstone causes a subsequent enrichment of Mg^{2+} and Fe^{2+}, which enter to the adjacent sandstone to occupy the remaining pores around calcites. This explains why the dolomites and ankerites always surround and replace calcites (Fig. 5A and B).

6. Conclusions

(1) Material sources of carbonate cements in the S-sandstones were mainly from the diagenetic alterations of nearby S-mudstones. Organic CO_2 derived from thermal evolution of organic materials in the S-mudstones participated during the precipitation process of carbonate cements in the S-sandstones. Carbonate cement content decreases gradually from the sharp contact to the center of the sandstone.
(2) Material sources of carbonate cements in the G-sandstones were mainly derived from the calcareous and clay matrix through in situ diagenetic alterations. Carbonate cement content decreases progressively from the gradual contact to the center of sandstone.
(3) Dissolution of feldspars and conversion of clay minerals provided the main material sources for the precipitation of carbonate cements in the center of sandstones. The precipitation temperatures of carbonate cements in both S-sandstones and G-sandstones are similar, lower than that of carbonate cements in the center of sandstones.
(4) Mass transfer of carbonate cements mainly occurred between the S-mudstones and the S-sandstones with limited transmission distance, which controlled the distribution of carbonate cements in the S-mudstones. There was almost no mass transfer between the G-mudstones and G-sandstones because of the small concentration gradient, instead, the depositional components and recrystallization controlled the carbonate distribution of the G-sandstones. Diagenesis in the S-mudstones had an apparently influence on the diagenesis of the adjacent S-sandstones, while diagenesis in the G-mudstones had little or no influence on diagenesis of the adjacent G-sandstones.

Acknowledgments

This work was co-funded by the Shandong Provincial Natural Science Foundation (ZR2019MD004), the National Natural Science Foundation of China (Grant No. U1762217, 418210002), the Fundamental Research Funds for the Central Universities of China (18CX05027A, 16CX02027A), the National Science and Technology Special of China (2017ZX05009001), and the Strategic Priority Research Program of the Chinese Academy of Sciences (Grant No. XDA14010301). We are also grateful to the Geosciences Institute of the Shengli Oilfield, SINOPEC, for permission to access their in-house database, providing background geologic data and permission to publish the results.

Appendix A. Supplementary data

Supplementary data to this article can be found online at https://doi.org/10.1016/j.marpetgeo.2019.07.005.

References

Friedman, I., O' Neil, 1977. Compilation of stable isotope fraction factors of geochemical interest. In: Fleischer, M. (Ed.), Data of Geochemistry, sixth ed. United States Geological Survey Professional Papers, pp. 440–1212.
Al-Aasm, I.S., Taylor, B.E., South, B., 1990. Stable isotope analysis of multiple carbonate samples using selective acid extraction. Chem. Geol. 80, 119–125.
Barth, T., Bjørlykke, K., 1993. Organic acids from source rock maturation: generation potentials, transport mechanisms and relevance for mineral diagenesis. Appl. Geochem. 8, 325–337.
Bjørlykke, K., 1993. Fluid flow in sedimentary basins. Sediment. Geol. 86, 137–158.
Bjørlykke, K., 1994. Fluid-flow processes and diagenesis in sedimentary basins. In: In: Parnell, J. (Ed.), Geofluid: Origin, Migration and Evolution of Fluids in Sedimentary Basins, vol. 78. Geol. Soc. (London) Spec. Publ., pp. 127–140.
Bjørlykke, K., 1996. Lithological control on fluid flow in sedimentary basins. In: Jamtveit, B., Yardley, B.W.D. (Eds.), Fluid Flow and Transport in Rocks: Mechanisms and Effect. Chapman and Hall, London, United Kingdom, pp. 15–34.
Bjørlykke, K., Aagaard, P., 1992. Clay minerals in north sea sandstones. In: In: Houseknecht, D.W., Pittman, E.D. (Eds.), Origin, Diagenesis and Petrophysics of Clay Minerals in Sandstones, vol. 47. SEPM Special Publication, pp. 65–80.
Bjørlykke, K., Jahren, J., 2012. Open or closed geochemical systems during diagenesis in sedimentary basins: constraints on mass transfer during diagenesis and the prediction of porosity in sandstone and carbonate reservoirs. AAPG Bull. 96, 2193–2214.
Boles, J.R., Franks, S.G., 1979. Clay diagenesis in Wilcox sandstones of southwest Texas: implications of smectite diagenesis on sandstone cementation. J. Sediment. Petrol. 49, 55–70.
Chen, D., Pang, X., Jiang, Z., Zeng, J., Qiu, N., Li, M., 2009. Reservoir characteristics and their effects on hydrocarbon accumulation in lacustrine turbidites in the Jiyang Super-depression, Bohai Bay Basin, China. Mar. Pet. Geol. 26, 149–162.
Day-Stirrat, R.J., Milliken, K.L., Dutton, S.P., Loucks, R.G., Hillier, S., Aplin, A.C., Schleicher, A.M., 2010. Open-system chemical behavior in deep wilcox group mudstones, Texas gulf coast, USA. Mar. Pet. Geol. 27, 1804–1818.
De Souza, R.S., De Assis Silva, C.M., 1998. Origin and timing of carbonate cementation of the Namorado sandstone (Cretaceous), Albacora Field, Brazil: implications for oil recovery. In: Morad, S. (Ed.), Carbonate Cementation in Sandstones. Blackwell Science, pp. 309–325.
Dos Anjos, S.M.C., De Ros, L.F., De Souza, R.S., De Assis Silva, C.M., Sombra, C.L., 2000. Depositional and diagenetic controls on the reservoir quality of Lower Cretaceous Pendência sandstones, Potiguar rift basin, Brazil. AAPG Bull. 84, 1719–1742.
Dutton, S.P., 2008. Calcite cement in Permian deep-water sandstones, Delaware Basin west Texas: origin, distribution, and effect on reservoir properties. AAPG Bull. 92, 765–787.
Dutton, S.P., Loucks, R.G., 2010. Diagenetic controls on evolution of porosity and permeability in lower Tertiary Wilcox sandstones from shallow to ultradeep (200-6700 m) burial, Gulf of Mexico Basin, USA. Mar. Pet. Geol. 27, 69–81.
Dutton, S.P., White, C.D., Willis, B.J., Novakovic, D., 2002. Calcite cement distribution and its effect on fluid flow in a deltaic sandstone, Frontier Formation, Wyoming. AAPG Bull. 86 2007–2021.
El-Ghali, M.A.K., Mansurbeg, H., Morad, S., Al-Aasm, I., Ajdanlisky, G., 2006. Distribution of diagenetic alterations in fluvial and paralic deposits within sequence stratigraphic framework: evidence from the petrohan terrigenous group and the svidol formation, lower triassic, NW Bulgaria. Sediment. Geol. 190, 299–321.
El-Ghali, M.A.K., Morad, S., Mansurbeg, H., Caja, M.A., Ajdanlijsky, G., Ogle, N., Al-Aasm, I., Sirat, M., 2009. Distribution of diagenetic alterations within depositional facies and sequence stratigraphic framework of fluvial sandstones: evidence from the Petrohan Terrigenous Group, Lower Triassic, NW Bulgaria. Mar. Pet. Geol. 26, 1212–1227.
El-Ghali, M.A.K., El Khoriby, E., Mansurbeg, H., Morad, S., Ogle, N., 2013. Distribution of carbonate cements within depositional facies and sequence stratigraphic framework of shoreface and deltaic arenites, Lower Miocene, the Gulf of Suez rift, Egypt. Mar. Pet. Geol. 45, 267–280.
Fayek, M., Harrison, T.M., Grove, M., McKeegan, K.D., Coath, C.D., Boles, J.R., 2001. In situ stable isotopic evidence for protracted and complex carbonate cementation in a petroleum reservoir, North Coles Levee, San Joaquin Basin, California, USA. J. Sediment. Res. 71, 444–458.
Folk, R.L., 1980. Petrology of Sedimentary Rocks. Hemphill Publishing, Austin, Texas, pp. 182.
Fontana, D., McBride, E.F., Kugler, R., 1986. Diagenesis and porosity evolution of submarine-fan and basin-plain sandstones, Marnoso-Arenacea Formation, northern Apennines, Italy. Bull. Can. Petrol. Geol. 34, 313–328.
Gaupp, R., Matter, A., Platt, J., Ramseyer, K., Walzabuck, J., 1993. Diagenesis and fluid

evolution of deeply buried Permian (Rotliegende) gas reservoirs, northwest Germany. AAPG Bull. 77, 1111–1128.
Guo, S., Tan, L., Lin, C., Li, H., Lu, X., Wang, H., 2014. Hydrocarbon accumulation characteristics of beach-bar sandstones in the southern slope of the dongying sag, Jiyang depression, Bohai Bay Basin, China. Petrol. Sci. 11, 220–233.
Hesse, R., Abid, I.A., 1998. In: In: Morad, S. (Ed.), Carbonate Cementation-The Key to Reservoir Properties of Four Sandstones Levels (Cretaceous) in the Hiberia Oil Field, Jeanne d'Arc Basin, Newfoundland, Canada. Carbonate Cementation in Sandstones, vol. 26. International Association of Sedimentologists Special Publication, pp. 363–394.
Holail, H.M., Kolkas, M.M., Friedman, G.M., 2006. Facies analysis and petrophysical properties of the lithologies of the north gas field. Qatar. Carbonate Evaporites 21, 40–50.
Jiang, Z., Liu, H., Zhang, S., Su, X., Jiang, Z., 2011. Sedimentary characteristics of large-scale lacustrine beach-bars and their formation in the Eocene boxing sag of Bohai Bay Basin, east China. Sedimentology 58, 1087–1112.
Karim, A., Pe-Piper, G., Piper, D.J.W., 2010. Controls on diagenesis of lower cretaceous reservoir sandstones in the western sable subbasin, offshore Nova Scotia. Sediment. Geol. 224, 65–83.
Kelts, K., Talbot, M.R., 1990. Lacustrine carbinates as geochemical archives of environmental change and biotic/abiotic interactions [C]. In: Tilzer, M.M., Serruya, C. (Eds.), Ecological Structure and Function in Large Lakes. Madison, Wis. Science Tech., pp. 290–317.
Kordi, M., Turner, B., Salem, A.M.K., 2011. Linking diagenesis to sequence stratigraphy in fluvial and shallow marine sandstones: evidence from the Cambrian-Ordovician lower sandstone unit in southwestern Sinai, Egypt. Mar. Pet. Geol. 28, 1554–1571.
Lampe, C., Song, G., Cong, L., Mu, X., 2012. Fault control on hydrocarbon migration and accumulation in the Tertiary Dongying depression, Bohai Basin, China. AAPG Bull. 96, 983–1000.
Land, L.S., 1983. The application of stable isotopes to studies of dolomite and to problems of diagenesis of clastic sediments. Stable Isotopes Sediment. Geol.: Soc. Econ. Palaeontol. Mineral. (short course) 10, 4 1–4.22.
Loyd, S.J., Corsetti, F.A., Eiler, J.M., Tripati, A.K., 2012. Determining the diagenetic conditions of concretion formation: assessing temperatures and pore waters using clumped isotopes. J. Sediment. Res. 82, 1006–1016.
Lynch, F.L., Land, L.S., 1996. Diagenesis of calcite cement in Frio sandstones and its relationship to formation water chemistry. J. Sediment. Res. 66, 439–466.
Macaulay, C.I., Haszeldine, R.S., Fallick, A.E., 1993. Distribution, chemistry, isotopic composition and origin of diagenetic carbonates; Magnus sandstone, North Sea. J. Sediment. Petrol. 63, 33–43.
Mansour, A.S., Rifai, R.I., Shaaban, M.N., 2014. Geochemical constraint on the origin of the multi-mineralogic carbonate cements in the subsurface Middle Jurassic sandstones, Central Sinai, Egypt. J. Geochem. Explor. 143, 163–173.
Mansurbeg, H., De Ros, L.F., Morad, S., Ketzer, J.M., El-Ghali, M.A.K., Caja, M.A., Othman, R., 2012. Meteoric-water diagenesis in late Cretaceous canyon-fill turbidite reservoirs from the Espirito Santo Basin, eastern Brazil. Mar. Pet. Geol. 37, 7–26.
McBride, E.F., Milliken, K.L., Cavazza, W., Cibin, U., Fontana, D., Picard, M.D., Zuffa, G.G., 1995. Heterogeneous distribution of calcite cement at the outcrop scale in Tertiary sandstones, northern Apennines, Italy. AAPG Bull. 79, 1044–1063.
McHargue, T.R., Price, R.C., 1982. Dolomite from clay in argillaceous limestones or shale associated marine carbonates. J. Sediment. Petrol. 52, 873–886.
McMahon, P.B., Chappele, F.H., Falls, W.F., Bradley, P.M., 1992. Role of microbial processes in linking sandstone diagenesis with organic-rich clays. J. Sediment. Petrol. 62, 1–10.
Merriman, R.J., 2005. Clay minerals and sedimentary basin history. Eur. J. Mineral. 17, 7–20.
Milliken, K.L., Land, L.S., 1993. The origin and fate of silt sized carbonate in subsurface Miocenee Oligocene mudstones, south Texas Gulf Coast. Sedimentology 40, 107–124.
Milliken, K.L., McBride, E.F., Cavazza, W., Cibin, U., Fontana, D., Picard, M.D., Zuffia, F.F., 1998. In: In: Morad, S. (Ed.), Geochemical History of Calcite Precipitation in Tertiary Sandstones, Northern Apennines, Italy: Carbonate Cementation in Sandstones, vol. 26. International Association of Sedimentologists Special Publication, pp. 213–240.
Rossi, C., Alaminos, A., 2014. Evaluating the mechanical compaction of quartzarenites: the importance of sorting (Llanos foreland basin, Colombia). Mar. Pet. Geol. 56, 222–238.
Rossi, C., Marfil, R., Ramseyer, K., Permanyer, A., 2001. Facies-related diagenesis and multiphase siderite cementation and dissolution in the reservoir sandstones of the Khatatba Formation, Egypt's Western Desert. J. Sediment. Res. 71, 459–472.
Rossi, C., Kalin, O., Arribas, J., Tortosa, A., 2002. Diagenesis, provenance and reservoir quality of triassic TAGI sandstones from ourhoud field, berkine (ghadames) basin, Algeria. Mar. Pet. Geol. 19, 117–142.
Rott, C.M., Qing, H., 2013. Early dolomitization and recrystallization in shallow marine carbonates, Mississippian Alida Beds, Williston Basin (Canada): evidence from petrography and isotope geochemistry. J. Sediment. Res. 83, 928–941.
Schultz, J.L., Boles, J.R., Tilton, G.R., 1989. Tracking calcium in the San Joaquin basin, California: a strontium isotopic study of carbonate cements at North Coles Levee. Geochem. Cosmochim. Acta 53, 1991–1999.
Sensula, B., Boettger, T., Pazdur, A., Piotrowska, N., Wagner, R., 2006. Carbon and oxygen isotope composition of organic matter and carbonates in recent lacustrine sediments. Geochronometria 25, 77–94.
Shew, R.D., 1990. Depositional and diagenetic controls on reservoir quality and gas composition in a mixed siliciclastic/carbonate setting, Thomasville field, Mississippi. AAPG Bull. 74, 762.
Surdam, R.C., Crossey, L.J., Sven Hagen, E., Heasler, H.P., 1989. Organic-inorganic and sandstone diagenesis. AAPG Bull. 73, 1–23.
Surdam, R.C., Jiao, Z., MacGowan, D.B., 1993. Redox reactions involving hydrocarbons and mineral oxidants; a mechanism for significant porosity enhancement in sandstones. AAPG Bull. 77, 1509–1518.
Thyne, G., 2001. A model for diagenetic mass transfer between adjacent sandstone and shale. Mar. Pet. Geol. 18, 743–755.
Udden, J.A., 1914. Mechanical composition of clastic sediments. Bull. Geol. Soc. Am. 25, 655–744.
Wang, J., Cao, Y., Liu, K., Liu, J., Xue, X., Xu, Q., 2016. Pore fluid evolution, distribution and water-rock interactions of carbonate cements in red-bed sandstone reservoirs in the Dongying Depression, China. Mar. Pet. Geol. 72, 279–294.
Wang, J., Cao, Y., Liu, K., Liu, J., Muhammad, K., 2017a. Identification of sedimentary-diagenetic facies and reservoir porosity and permeability prediction: an example from the Eocene beach-bar sandstone in the Dongying Depression, China. Mar. Pet. Geol. 82, 69–84.
Wang, J., Cao, Y., Song, G., Liu, H., 2017b. Diagenetic evolution and formation mechanisms of high-quality reservoirs under multiple diagenetic environmental constraints: an example from the paleogene beach-bar sandstone reservoirs in the dongying depression, Bohai Bay Basin. Acta Geol. Sin. Engl. 91, 232–248.
Wang, J., Cao, Y., Liu, K., Costanzo, A., Feely, M., 2018. Diagenesis and evolution of the lower Eocene red-bed sandstone reservoirs in the Dongying Depression, China. Mar. Pet. Geol. 94, 230–245.
Wang, J., Cao, Y., Xiao, J., Liu, K., Song, M., 2019. Factors controlling reservoir properties and hydrocarbon accumulation of the Eocene lacustrine beach-bar sandstones in the Dongying Depression, Bohai Bay Basin, China. Mar. Pet. Geol. 99, 1–16.
Wentworth, C.K., 1922. A scale of grade and class terms for clastic sediments. J. Geol. 30, 377–392.
Wenzel, B., 2000. Differential preservation of primary isotopic signatures in silurian brachiopods from northern Europe. J. Sediment. Res. 70, 194–209.
Zhang, C., Jiang, Z., Zhang, Y., Chen, Q., Zhao, W., Xu, J., 2012. Reservoir characteristics and its main controlling factors of the siegenian formation of devonian in X block, Algeria. Energy Explor. Exploit. 30, 727–751.